Noncollocated Control of Distributed-Parameter Nondispersive Systems with Tip Inertias Using Time Delays

Firdaus E. Udwadia

Mechanical and Civil Engineering Departments
University of Southern California
430K Olin Hall
Los Angeles, California 90089-1453

ABSTRACT

This paper deals with the noncollocated, time-delayed active point control of a spatially finite system which has a tip inertia and which is modeled by the one-dimensional wave equation. The paper presents a new method of control of the system using noncollocated sensors and actuators. By using the physical properties of the mode shapes of vibration of the system it is shown that the modal response at a given location in the system can be reconstructed from the *time-delayed* modal responses at (at most) three different locations in the system. Based on this observation, a closed-loop control design is provided which is capable of stabilizing the system and dampening the vibrations in all its modes, while using dislocated sensor and actuator locations. Simple finite-dimensional controllers are used in the control design. Explicit conditions are provided to obtain the bounds on the controller gains to ensure stability of the closed-loop control design. These bounds are obtained in terms of the locations of the sensors and the actuators. Simulation results, which validate the control methodology and the theoretical bounds on the gain, are also presented.

INTRODUCTION

The control of distributed systems is an active area of current research. It has wide-ranging applications in the fields of aerospace engineering, mechanical engineering, civil engineering, and petroleum engineering. The control of large space structures for vibration suppression and pointing controls, the control of rotors and shafts and mechanical assemblies, active control of buildings subjected to earthquakes, and the control of oil recovery from natural reservoirs are some examples (see, for example, [4, 6, 2, 9, 7, 10, 1, 13–15]).

APPLIED MATHEMATICS AND COMPUTATION 47:47–75 (1992)

655 Avenue of the Americas, New York, NY 10010

0096-3003/92/$03.50

In this paper we consider systems which are of finite spatial extent and which can be modeled by the one-dimensional undamped wave equation. The paper is an extension of previous work [15] in that it concerns itself with systems with tip inertias. Situations where tip inertia is important in the proper modeling of structural systems constitute an important class of problems in themselves. Furthermore, the presence of the tip inertia substantially changes the results as well as the derivations from those obtained previously. *We show that noncollocated point control of such a neutrally stable distributed system, using finite-dimensional controllers, can lead to complete controllability of the system without any spillover effects.* It is shown that a large variety of simple and commonly used controllers, among them velocity-feedback controllers and lead-lag compensators, can adequately perform the task. This is achieved by the judicious placement of sensors in the system and the acquisition of data from those locations with specific time delays. While it has been known for some time that collocated control (where the sensor and actuator are placed at the same location) leads to complete controllability of the system [6], with no spillover, similar results for noncollocated systems are rare (see [14]). In fact, it is known that noncollocation of sensors and actuators generally results in loss of controllability due to spillover effects.

In Section I of this paper we introduce some basic preliminaries and develop the open-loop Green's function for the system. Section II deals with some key properties of the mechanical responses of such a system and the determination of sensor and actuator locations. Section III deals with closed-loop feedback control, the associated Green's functions, and the closed-loop transfer function for the distributed system. Section IV deals with stability issues and provides explicit bounds for the controller gain to ensure controllability. Section V presents some simulation results, and Section VI gives the conclusions.

I. SYSTEM MODEL

Consider a spatially distributed system subjected to a time-varying force $f(x,t)$ described by

$$z_{tt} = c^2 z_{xx} + f(x,t), \tag{1}$$

where the space parameter x extends from 0 to L. The wave speed in the medium is denoted by c, and $f(x,t)$ is the force normalized with respect to the inertial mass per unit length of the medium. The subscripts t and x refer to differentiation with respect to time t and space x. This equation,

though simplistic, governs the motion $z(x,t)$ of diverse systems: the torsional vibrations of bars, the axial vibrations of rods, the horizontal motions of buildings, etc. We shall assume that the boundary conditions are given by

$$z_x(0,t) - h_1 z(0,t) = 0 \tag{2}$$

and

$$z_x(L,t) + h_2 z_{tt}(L,t) = 0 \tag{3}$$

and that the initial conditions are $z_t(x,0) = z(x,0) = 0$.

For a uniform bar (see Figure 1) which is elastically restrained at one end and which is undergoing axial vibrations, $c^2 = E/\rho$, where E is the Young's modulus, A is the cross-sectional area of the bar, and ρ is the density. The parameter h_1 is then given by the ratio k_0/EA, where k_0 is the spring constant of the restraint at the left-hand end. We shall assume throughout this paper that h_1 is positive. The parameter h_2 in Equation (3) then represents M_{tip}/mc^2, where M_{tip} is the magnitude of the tip mass and m ($= A\rho$) is the mass per unit length of the bar. Similar interpretations for the torsion problem can be adduced. The eigenvalue problem related to Equations (1)–(3) can be written as

$$u_{xx} + \beta^2 u = 0, \qquad \beta^2 = \frac{\omega^2}{c^2}, \tag{4}$$

with

$$u_x(0) - h_1 u(0) = 0 \tag{5}$$

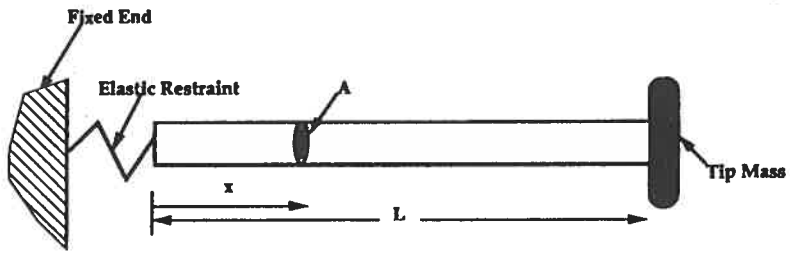

FIG. 1. A uniform bar of density ρ, cross section A, and length L, modeled by Equations (1)–(3) with an elastic restraint at one end and a tip mass M_{tip} at the other.

and

$$u_x(L) - M_r\beta^2 u(L) = 0, \tag{6}$$

where the mass ratio is given by $M_r = M_{tip}/m$. The general solution of (4) is

$$u(x) = A\cos\beta x + B\sin\beta x = C\sin(\beta x + \phi), \tag{7}$$

where A and B are constants. Using (5), we obtain

$$u(x) = B\left[\frac{\beta}{h_1}\cos\beta x + \sin\beta x\right], \tag{8}$$

and using (6), we obtain the natural frequencies of vibration of the system from the roots of the equation

$$\tan\beta L = \frac{h_1 - \beta^2 M_r}{\beta[1 + h_1 M_r]} \tag{9}$$

The roots β_n of Equation (9) are all real, and they provide the countably infinite set of eigenvalues of the system described by Equations (4), (5), and (6). We shall denote them by $\beta_1, \beta_2, \ldots$. The corresponding eigenfunctions may be found as

$$u_n = \frac{\beta}{h_1}\cos\beta_n x + \sin\beta_n x, \tag{10}$$

or

$$u_n = \sin(\beta_n x + \phi_n), \tag{11}$$

where

$$\phi_n = \tan^{-1}\frac{\beta_n}{h_1}. \tag{12}$$

Furthermore, there are no repeated eigenvalues. We note the following:

(a) When $h_1 \to \infty$, the end $x = 0$ is fixed and $\phi_n = 0$. Thus $u_n = \sin\beta_n x$ and the characteristic equation becomes

$$\tan\beta_n L = \left(\frac{1}{\beta M_r}\right).$$

(b) When $h_1, M_r \to \infty$, we have a fixed-free system, the eigenfunction becomes $u_n = \sin\beta_n x$, $\phi_n = 0$, and the eigenvalues are $\beta_n = n\pi/L$, $n = 1, 2, \ldots$.

(c) When $h_1 \to \infty$, $M_r \to 0$, we have a fixed-free system and the eigenfunctions are

$$u_n = \sin\beta_n x, \quad \beta_n = \frac{(2n-1)\pi}{2L}, \qquad n = 1, 2, \ldots.$$

(d) The eigenfunctions of Equation (4) are always of the form

$$u_n = \sin(\beta_n x + \phi_n).$$

The boundary conditions (values of h_1 and M_r) affect the eigenvalues β_n and the phase angle ϕ_n.

Taking Laplace transforms and denoting the transform variable by s, the solution to Equations (1)–(3) can be obtained using the Green's function (see [12]) as

$$z(x, s) = \int_0^L g_0(x, \xi, s) f(\xi, s)\, d\xi, \tag{13}$$

where

$$g_0(x, \xi, s) = \begin{cases} \dfrac{\sinh(\bar{\beta}\xi + \bar{\psi})\sinh(\bar{\beta}x + \bar{\phi})}{\bar{\beta}c^2\sinh(\bar{\psi} - \bar{\phi})}, & x \leqslant \xi, \\ \dfrac{\sinh(\bar{\beta}\xi + \bar{\phi})\sinh(\bar{\beta}x + \bar{\psi})}{\bar{\beta}c^2\sinh(\bar{\psi} - \bar{\phi})}, & x \geqslant \xi, \end{cases} \tag{14}$$

with $s^2 = c^2\bar{\beta}^2$, and

$$\tanh\bar{\phi} = \frac{\bar{\beta}}{h_1}, \tag{15a}$$

$$\tanh\bar{\psi} = -\frac{M_r\bar{\beta}^2\sinh\bar{\beta}L + \bar{\beta}\cosh\bar{\beta}L}{\bar{\beta}\sinh\bar{\beta}L + M_r\bar{\beta}^2\cosh\bar{\beta}L}. \tag{15b}$$

The open-loop transfer frunction $g_0(x, \xi, s)$ has an infinite number of poles at $s = \pm i\omega_n$. All these poles lie on the imaginary axis in the s-plane.

II. DETERMINATION OF SENSOR AND ACTUATOR PLACEMENTS

We begin by noting that the eigenfunction response of the system governed by Equations (1)–(3) looks like

$$u_n(x,t) = \sin(\beta_n x + \phi_n)\, e^{i\omega_n(t+\psi_n)}, \tag{16}$$

which can be expressed as

$$u_n(x,t) = \frac{e^{i(\beta_n x+\phi_n)} - e^{-i(\beta_n x+\phi_n)}}{2i} \times e^{ic\beta_n(t+\psi_n)}. \tag{17}$$

Furthermore for any location $x_1 > x_2$ we have

$$u_n\left(x_1, t-\frac{x_2}{c}\right) - u_n\left(x_2, t-\frac{x_1}{c}\right) = u_n(x_1-x_2,t) - e^{-i\beta_n(x_1-x_2-ct)} \sin\phi_n\, e^{i\omega_n\psi_n}, \tag{18}$$

and similarly, for any location $x_a > x_3$ we get

$$u_n\left(x_a, t-\frac{x_3}{c}\right) - u_n\left(x_3, t-\frac{x_a}{c}\right) = u_n(x_a-x_3,t) - e^{-i\beta_n(x_a-x_3-ct)} \sin\phi_n\, e^{i\omega_n\psi_n}. \tag{19}$$

The subscript a on x denotes, as we shall see in the next section, the actuator location. If we further choose the locations $x_a > x_3$ such that $x_1 - x_2 = x_a - x_3$ and subtract Equation (19) from (18), we obtain

$$u_n\left(x_a, t-\frac{x_3}{c}\right) = u_n\left(x_1, t-\frac{x_2}{c}\right) + u_n\left(x_3, t-\frac{x_a}{c}\right) - u_n\left(x_2, t-\frac{x_1}{c}\right), \qquad \forall n, \forall t. \tag{20}$$

Without loss in generality we can choose $x_a < x_1$ so that $x_3 < x_2$. Then

time-shifting Equation (20) by x_3/c, we get

$$u_n(x_a,t) = u_n(x_1, t-T_1) + u_n(x_3, t-T_3) - u_n(x_2, t-T_2), \tag{21}$$

where

$$T_1 = \frac{x_2 - x_3}{c}, \qquad T_2 = \frac{x_1 - x_3}{c}, \qquad T_3 = \frac{x_a - x_3}{c}. \tag{22}$$

The time delays T_1, T_2, T_3 are all positive, and thus we have been able to obtain a perfect "predictor" for the nth-mode response at location x_a at time t by looking at the nth-mode response at locations x_1, x_2, and x_3 at times $t - T_1$, $t - T_2$, and $t - T_3$ respectively. To predict the response of the nth mode ($n = 1, 2, \ldots$) at location x_a we therefore need, in general, *three sensors*. We note that $x_1 - x_2 = x_a - x_3$. The location of x_a relative to x_2 is left open for now. Two possible configurations could arise. We shall refer to them as:

(a) configuration C1, when $x_3 < x_a < x_2 < x_1$, and
(b) configuration C2, when $x_3 < x_2 < x_a < x_1$.

For both these conditions, the relations (21) and (22) are valid. In Section V we shall see however that there is some difference in these two configurations in that they lead to different bounds on the controller gains to ensure stability.

We note the following:

(a) Since the time delays T_1, T_2, T_3 in Equations (21) and (22) do not involve the mode numbers, the same three locations and the same three delays will provide predictions for all modes.

(b) When $\phi_n = 0$ ($h_1 \to \infty$), Equation (21) yields, for $x_1 > x_a$,

$$u_n(x_a,t) = u_n\left(x_1, t-\frac{x_2}{c}\right) - u_n\left(x_1 - x_a, t-\frac{x_1}{c}\right) \qquad \forall n, \forall t. \tag{21'}$$

Thus to predict the nth-mode response at time t at location x_a we need sensors at locations x_1 and at $x_2 = x_1 - x_a$. Data on the nth mode obtained at times $t - x_2/c$ and $t - x_1/c$ respectively yield perfect predictions of the nth-mode response at location x_a at time t. Since the time delays are independent of the mode number, these statements are true for any mode.

(c) For the fixed-fixed system($h_1, M_r \to \infty$), we obtain

$$u_n(x_a,t) = -u_n\left(L - x_a, t-\frac{L}{c}\right) \qquad \forall n, \forall t. \tag{21''}$$

Thus one sensor located at $L - x_a$ will predict $u_n(x_a, t)$, $n = 1, 2, \ldots$.

In the same manner as for Equation (21), we can show that

$$u_n(x_a) = u_n(x_1)e^{\pm i\omega_n T_1} + u_n(x_3)e^{\pm i\omega_n T_3} - u_n(x_2)e^{\pm i\omega_n T_2} \qquad \forall n. \quad (23)$$

This result is valid for all modes n. It is physically indicative of the fact that the response of the nth mode at a location x_a and time t can be precisely predicted by the response at three locations x_1, x_2, x_3 with appropriate time delays T_1, T_2, and T_3. We shall use this important result later in Section IV and in a proof presented in the appendix.

III. CLOSED-LOOP CONTROL

We can now design a feedback controller for the distributed system of Equation (1), where the location x_a of the actuator is chosen so that: (a) it does not lie on any node of any mode of the system, and (b) $x_1 - x_2 = x_a - x_3$.

Figure 2 shows the control design. The sensors, which are located at x_1, x_2, x_3, are polled, as shown in the figure, at time delays of T_1, T_2, and T_3 respectively. The outputs from the sensors located at x_1 and x_3 are added together, those from x_2 are subtracted, and the combined signal is multiplied by minus one and then fed to a finite-dimensional controller. The controller has a transfer function of $\mu\mathcal{T}_c(s) := \mu K(s)/P(s)$, where μ is the controller gain. We shall assume, in what follows, that $K(i\omega) \neq 0$ for all ω.

Using Equation (13) and letting $f(\xi, s) = f_d(\xi, s) - f_c(u, s)$, where f_c represents the feedback control force and f_d the disturbance, we obtain

$$z(x, s) = \int_0^L g_0(x, \xi, s)\left[f_d(\xi, s) - f_c(\xi, s)\right] d\xi. \qquad (24)$$

Using an actuator at location x_a we obtain (see Figure 2)

$$f_c(\xi, s) = \mu\mathcal{T}_c(s)\left[z(x_1, s)e^{-sT_1} - z(x_2, s)e^{-sT_2} + z(x_3, s)e^{-sT_3}\right]\delta(\xi - x_a). \qquad (25)$$

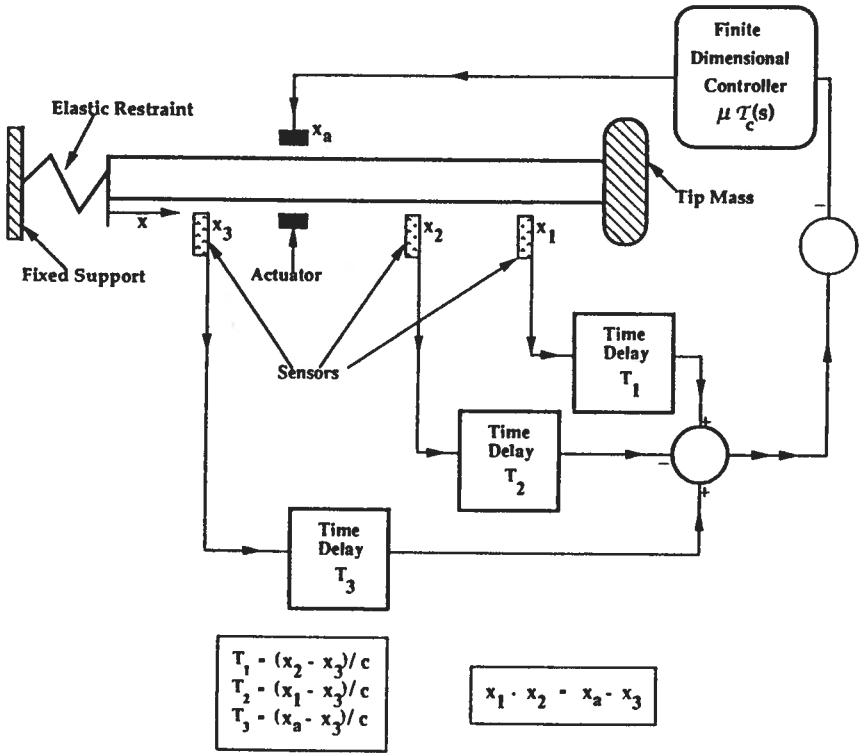

FIG. 2. Noncollocated time-delayed control design, showing three sensors at locations x_1, x_2, and x_3, and an actuator at location x_a. The arrangement corresponds to configuration C1.

Equation (25) then becomes

$$z(x, s) = \int_0^L g_0(x, \xi, s)f_d(\xi, s)\, ds - g_0(x, x_a, s)\mu\mathcal{T}_c(s)\left[z(x_1, s)e^{-sT_1} - z(x_2, s)e^{-sT_2} + z(x_3, s)e^{-sT_3}\right] \qquad (26)$$

Denoting

$$\alpha(x, x_a, s) = \mu\mathcal{T}_c(s)g_0(x, x_a, s), \qquad (27)$$

$$F_d(x,s) = \int_0^L g_0(x,\xi,s) f_d(\xi,s)\, d\xi, \tag{28}$$

$$\underline{\mathscr{F}}(s) = \left[F_d(x_1,s) \quad F_d(x_2,s) \quad F_d(x_3,s) \right]^T, \tag{29}$$

$$\underline{G}_0(\xi,s) = \left[g_0(x_1,\xi,s) \quad g_0(x_2,\xi,s) \quad g_0(x_3,\xi,s) \right]^T, \tag{30}$$

$$\underline{d} = \left[e^{-sT_1} \quad -e^{-sT_2} \quad e^{-sT_3} \right]^T, \tag{31}$$

$$\underline{\mathscr{Z}}(s) = \left[z(x_1,s) \quad z(x_2,s) \quad z(x_3,s) \right]^T, \tag{32}$$

Equation (26) can be rewritten as

$$z(x,s) = F(x,s) - \alpha(x,x_a,s)\underline{d}^T \underline{\mathscr{Z}}(s). \tag{33}$$

Letting $x = x_1$, x_2, and x_3 in (33) yields the set of simultaneous equations

$$A\underline{\mathscr{Z}} = \underline{\mathscr{F}}, \tag{34}$$

where

$$A = \begin{bmatrix} 1+\alpha(x_1,x_a,s)e^{-sT_1} & -\alpha(x_1,x_a,s)e^{-sT_2} & \alpha(x_1,x_a,s)e^{-sT_3} \\ \alpha(x_2,x_a,s)e^{-sT_1} & 1-\alpha(x_2,x_a,\omega)e^{-sT_2} & \alpha(x_2,x_a,s)e^{-sT_3} \\ \alpha(x_3,x_a,s)e^{-sT_1} & -\alpha(x_3,x_a,s)e^{-sT_2} & 1+\alpha(x_3,x_a,s)e^{-sT_3} \end{bmatrix}. \tag{35}$$

This yields

$$\underline{\mathscr{Z}} = A^{-1}\underline{\mathscr{F}}, \tag{36}$$

so that (33) becomes

$$z(x,s) = F(x,s) - \alpha(x,x_a,s)\underline{d}^T A^{-1}\underline{\mathscr{F}}. \tag{37}$$

We next present two properties of the matrix A which can be directly verified:

$$\begin{aligned} \det A &= 1 + \alpha(x_1,x_a,s)e^{-sT_1} - \alpha(x_2,x_a,s)e^{-sT_2} + \alpha(x_3,x_a,s)e^{-sT_3} \\ &= 1 + \mu\mathscr{T}_c(s)\underline{d}^T(s)\underline{G}_0(x_a,s), \end{aligned} \tag{38}$$

and

$$d^T A^{-1} = \frac{1}{\det A} d^T. \tag{39}$$

We then obtain for the closed-loop response

$$\begin{aligned} z(x,s) = \frac{1}{\det A}\int_0^L \big[&(\det A)\, g_0(x,\xi,s) \\ &- \alpha(x,x_a,s)\underline{d}^T\underline{G}_0(\xi,s) \big] f_d(\xi,s)\, d\xi, \end{aligned} \tag{40}$$

and for the closed-loop transfer function

$$G_{cl}(x,\xi,s) = \left[\frac{(\det A)\, g_0(x,\xi,s) - \alpha(x,x_a,s)\underline{d}^T\underline{G}_0(\xi,s)}{\det A} \right]. \tag{41}$$

The closed-loop poles lie at the roots of

$$\begin{aligned} \det A = 1 + \mu\mathscr{T}_c(s)\big[&g_0(x_1,x_a,s)e^{-sT_1} + g_0(x_3,x_a,s)e^{-sT_3} \\ &- g_0(x_2,x_a,s)e^{-sT_2} \big] = 0. \end{aligned} \tag{42}$$

We next consider stability of the control design.

IV. STABILITY AND CONTROLLER DESIGN

1. *Stability for Small Gains* μ

To study the stability of the control design, we shall use the following stability criterion. Noting that the open-loop poles occur at the frequencies $s_k = \pm i\omega_k$ where ω_k is real, we see that the root locus $s_k(\mu)$ of the kth closed-loop pole, which starts for $\mu = 0$ at ω_k on the imaginary axis,

will move to the left half s-plane if

$$\mathrm{Re}\left\{\frac{ds_k}{d\mu}\right\}_{\mu=0+} < 0 \qquad \forall k. \tag{43}$$

If this condition is satisfied, then for vanishingly small and positive values of μ, all the closed poles will have negative real parts and control will therefore be stable. Substituting the expression for the Green's function $g_0(x_i, x_a, s)$, $i = 1,2,3$, obtained in (14) into Equation (42), we obtain the following for the two configurations C1 and C2:

$$1 + \mu \mathscr{T}_c(s)\left[g_0(x_a, x_a, s) - \frac{e^{-\bar{\beta}(x_a - x_3)}}{\bar{\beta}c^2}\sinh\bar{\beta}(x_a - x_3)\right] = 0 \qquad \text{for C1,} \tag{44}$$

and

$$1 + \mu \mathscr{T}_c(s)\left[g_0(x_a, x_a, s) - \frac{e^{-\bar{\beta}(x_2 - x_3)}}{\bar{\beta}c^2}\sinh\bar{\beta}(x_2 - x_3)\right] = 0 \qquad \text{for C2,} \tag{45}$$

where

$$x_1 - x_2 = x_a - x_3 \quad \text{and} \quad s^2 = c^2\bar{\beta}^2. \tag{46}$$

This yields

$$\left.\frac{d\bar{\beta}}{d\mu}\right|_{\mu=0+,\ \bar{\beta}=\to \pm i\omega_k/c} = \frac{1}{d(\bar{\psi}-\bar{\phi})/d\beta|_{\bar{\beta}=\to \pm i\omega_k/c}} \times \frac{\sin(\omega_k x_a/c+\phi)\sin(\omega_k x_a/c+\phi\pm n\pi)}{c\cos(\pm n\pi)} \lim_{s\to \pm i\omega_k}\frac{\mathscr{T}_c(s)}{s}, \tag{47}$$

where, in going from (45) and (46) to (47), we have made use of the

following notation and results:

(1) $\bar{\psi} = i\psi$ and $\bar{\phi} = i\phi$.

(2) At $\bar{\beta} = \pm i\omega_k/c$, where ω_k is an open-loop pole, $\sinh(\bar{\psi} - \bar{\phi}) = 0$ [see Equation (14)] and hence $\psi = \phi \pm n\pi$.

Using Equation (15), we show in Appendix 1 that

$$\left.\frac{d(\bar{\psi}-\bar{\phi})}{d\bar{\beta}}\right|_{\bar{\beta}=\to \pm \frac{i\omega_k}{c}} = -\gamma_k,$$

where γ_k is a positive real number. Thus we obtain

$$\left.\frac{ds}{d\mu}\right|_{\mu=0+,\ s=\to \pm i\omega_k} = -\frac{\sin^2(\omega_k x_a/c+\phi)}{\gamma_k}\lim_{s\to \pm i\omega_k}\frac{\mathscr{T}_c(s)}{s}, \tag{48}$$

so that for the condition (43) to be satisfied we require

$$\mathrm{Re}\lim_{s\to \pm i\omega_k}\frac{\mathscr{T}_c(s)}{s} > 0 \qquad \text{for all } k. \tag{49}$$

Note that the $\sin^2$ term in Equation (48) cannot be zero, because x_a is not at any node of any mode of the open-loop system. Taking the transfer function of the controller to be

$$\mathscr{T}_c(i\omega) := \frac{K(i\omega)}{P(i\omega)} = a(\omega) + ib(\omega), \tag{50}$$

where $K(i\omega)$ and $P(i\omega)$ are polynomials, the condition (49) requires that at *each* open-loop pole,

$$\lim_{\omega\to \pm \omega_k}\frac{b(\omega)}{\omega} > 0, \qquad k = 1,2,\ldots,\infty. \tag{51}$$

If we choose $b(\omega)$ to be a continuous function, we then need it to be an *odd* function of ω, with $b(0) = 0$, $b(\omega) > 0$, $\omega\in(0,\infty)$. *Throughout this paper we will assume that $b(\omega)$ of the controller's transfer function has this property.* Let us denote this property by P1. Examples of a few such simple finite-dimensional controllers are:

(1) a velocity-feedback controller with

$$\mathscr{T}_c(i\omega) = i\omega, \tag{52}$$

(2) a lag-lead compensator (with more lead than lag),

$$\mathcal{F}_c(i\omega) = \frac{1+i\omega\tau_1}{1+i\omega\tau_2}, \qquad \tau_1 > \tau_2 > 0. \tag{53}$$

We have so far proved stability when the controller gain μ is positive, though it may be vanishingly small.

While we have dealt with the general boundary-condition situation, the results on the stability of the closed-loop system when $\phi_n = 0$ and two sensors are used follow *mutatis mutandis*. The closed-loop transfer function is stable, and controllers such as the two mentioned above in Equations (52)–(53) will bring about stabilization of the system for vanishingly small gains.

2. *The Development of an Upper Bound $\mu^{\max}$ for the Controller Gain*

Let us denote by $\mu^{\max}$ the upper bound on μ up to which the closed-loop control described in this paper is stable. In this subsection we show that one can actually provide explicit expressions for a parameter M, $M > 0$, such that $\mu^{\max} \geqslant M$ for the closed-loop, time-delayed, noncollocated system to be stable when the controller's transfer function $\mathcal{F}_c$ satisfies property P1.

We have shown that the closed-loop poles are obtained as the roots of Equations (44) and (45), depending on whether configuration C1 or C2 is used. We have shown stability for (infinitesimally) small positive gains when the controller's transfer function $\mathcal{F}_c(i\omega) := a(\omega) + ib(\omega)$ is such that property P1 is satisfied. In that case the root locus of every closed-loop pole, for infinitesimal gains, will move towards the left half s-plane. We observe that before the root locus of any pole bends back and moves into the right half s-plane it would have to cross the imaginary axis.

Let us say that the root locus bends back and crosses the imaginary axis at $s = \pm i\eta$. Then, setting the real and imaginary parts of Equations (44a) and (44b), at $s = \pm i\eta$, to zero, we find that one of the conditions that we require is

$$\sin^2 \frac{\pm \eta y}{c} = \frac{c}{\mu}\left(\frac{\eta b(\eta)}{a^2(\eta) + b^2(\eta)}\right), \tag{54}$$

where $y = x_a - x_3$ for configuration C1, and $y = x_2 - x_3$ for configuration C2. The quantities $a(\eta)$ and $b(\eta)$ are the real and imaginary parts of the controller's transfer function at $s = i\eta$.

A. Stability Bound When $a(0) > 0$. Consider the class of controllers for which $a(0) > 0$, so that $\mathcal{F}_c(0) > 0$. Many commonly used controllers fall

in this category [e.g., Equation (53)]. Then Equation (54) is satisfied when $\eta = 0$. This corresponds to a value of μ given by (we assume that the appropriate limits exist, i.e., no rigid-body modes)

$$\frac{1}{\mu\,\mathcal{F}_c(0)} = -\left[\lim_{s\to 0} g_0(x_a, x_a, s) - \frac{y}{c^2}\right], \tag{55}$$

where again, $y = x_a - x_3$ for configuration C1, and $y = x_2 - x_3$ for configuration C2. But the value of $\lim_{s\to 0} g_0(x_a, x_a, s)$ for the problem (1)–(3) is given by $(1/c^2)[x_a + (1/h_1)]$. This follows directly from the Green's function, in which we use (14) and (15). Hence,

$$\lim_{s\to 0}\{g_0(x_a, x_a, s\} > \frac{x_a - x_3}{c^2} \qquad \text{for C1,} \tag{56a}$$

and

$$\lim_{s\to 0}\{g_0(x_a, x_a, s\} > \frac{x_2 - x_3}{c^2} \qquad \text{for C2.} \tag{56b}$$

Thus the values of μ obtained in (55) would be negative and would therefore be irrelevant to obtaining a bound on it. (Note that when h_1 is zero, the Green's function is unbounded for $\beta \to 0$. This is because we then have a rigid-body mode in the open-loop system, whose natural frequency is zero.)

Furthermore, the left-hand side of Equation (54) has a maximum value of unity when

$$\eta_k^* = \pm \frac{(2k-1)\pi c}{2(x_a - x_3)}, \quad k = 1, 2, \ldots, \qquad \text{for configuration C1,} \tag{57a}$$

and

$$\eta_k^* = \pm \frac{(2k-1)\pi c}{2(x_2 - x_3)}, \quad k = 1, 2, \ldots, \qquad \text{for configuration C2.} \tag{57b}$$

We can then ensure that Equation (54) will *not* be satisfied by choosing a μ such that

$$\frac{c}{\mu}\left[\frac{\eta b(\eta)}{a^2(\eta) + b^2(\eta)}\right] > \sin^2 \frac{\pm \eta y}{c} \qquad \text{for all } \eta. \tag{58}$$

When the quantity in brackets on the left-hand side of Equation (58) is a monotone function, a bound M for $\mu^{\max}$ can often be found by ensuring

that the left-hand side is greater than unity at η_1^*. This yields (see Section V.2)

$$\mu^{\max} \geqslant M = \frac{\eta_1^* b(\eta_1^*)}{a^2(\eta_1^*) + b^2(\eta_1^*)} \cdot c, \tag{59}$$

where η_1^* is as defined in Equation (57) for the two configurations C1 and C2. Note that the condition (58) ensures that the root locus does not bend back and cut the imaginary axis. As indicated in Equation (59), the upper bound on μ for stability could, in general, be greater than M; for, even when $\mu > M$, the root locus may still *not* cross the imaginary axis. We have thus obtained a lower bound on $\mu^{\max}$. Stability is ensured for $0 < \mu < M \leqslant \mu^{\max}$. In the next section we show some numerical examples where the value of M obtained by Equation (59) is not too far from $\mu^{\max}$.

We note from (59) that the value of M, when Equation (56) is satisfied, is dependent *only* on (1) the nature of the controller's transfer function, (2) the wave speed in the medium, c, and (3) the separation distance: $x_a - x_3$ for C1, and $x_2 - x_3$ for C2.

B. Stability Bound for Velocity Feedback Control. When we use velocity feedback [$a(i\omega) = 0$, $b(i\omega) = \omega$ for all ω], we observe that the right-hand side of Equation (54) is now a constant whose value is c/μ. Furthermore, this equation cannot be satisfied as long as $\mu < c$; hence $M = c$. The exact upper bound for μ must therefore satisfy the equation

$$1 + \mu \mathcal{T}_c(\bar{\beta}^* c)\left[g_0(x_a, x_a, s) - \frac{e^{-\bar{\beta}^* y}}{c^2 \bar{\beta}^*} \sinh \bar{\beta}^* y \right] = 0, \tag{60}$$

with $y = x_a - x_3$ for configuration C1, and $y = x_2 - x_3$ for configuration C2 and,

$$\bar{\beta}_n^* = \pm \frac{i}{y}\left(n\pi \pm \sin^{-1}\sqrt{\frac{c}{\mu}} \right) \tag{61}$$

where $n = 0, 1, 2, 3, \ldots$. This follows from Equations (54) and (44). The smallest positive root of Equation (60), for any given $\mathcal{T}_c$, then yields $\mu^{\max}$. We will show some numerical examples in the next section.

C. Collocated Sensors and Actuators: A Special Case of Noncollocation. Were we to *collocate* the sensor and the actuator, i.e., use one sensor and place it at the actuator location x_a, then the system described by Equation (1) could be stabilized by any controller whose transfer function $\mathcal{T}_c$ satisfies property P1 and for which $a(0) \geqslant 0$. We show here why this is true.

A collocated actuator-and-sensor pair becomes a special case of the control $f_c(\xi, s)$ described in Equation (28) when $x_1 = x_2 = x_3 = x_a$ and $T_1 = T_2 = T_3 = 0$. Results obtained earlier can therefore be particularized by making these substitutions in the expressions. In particular, the closed-loop transfer-function poles for collocation of sensors and actuators can be obtained from Equation (42) by setting $x_1 = x_2 = x_3 = x_a$ and $T_i = 0$, $i = 1, 2, 3$. The matrix A [see Equation (29)] now reduces to a scalar. Denoting this scalar by $A^{(\mathrm{col})}$ for the collocated case, we obtain, using Equations (42) and (44), the closed-loop poles from the following condition:

$$\det A^{(\mathrm{col})} = 1 + \mu \mathcal{T}_c(s) g_0(x_a, x_a, s) = 0. \tag{62}$$

The derivative $ds_k/d\mu|_{\mu=0+}$ can be obtained as before, and is given again by the expression in Equation (48). The fact that this expression is the same as for the noncollocated situation indicates that as μ increases from zero, the poles begin to move for the collocated case in exactly the same way as they do for our dislocated control design with proper time delays; this points out that in some sense, for vanishingly small gains, the dislocation when done properly is tantamount to a collocation. Thus as long as the transfer function of the controller satisfies property P1, the root loci of all the poles s_k will move to the left half of the s-plane for infinitesimally positive values of μ.

Thus, for the root locus of any pole to move into the positive half s-plane, we would require that it cut the imaginary axis at some $s = \pm i\eta$. Hence, for the closed-loop control to lose stability for some value of μ, Equation (62) must be satisfied for $s = \pm i\eta$. This requires, for $\mu > 0$, that

$$\frac{1}{\mu} + a(i\eta) g_0(x_a, x_a, i\eta) + ib(i\eta) g_0(x_a, x_a, i\eta) = 0. \tag{63}$$

If $g(x_a, x_a, i\eta) = 0$, Equation (63) cannot be satisfied [we assume that $b(i\eta)$ is bounded]. Let

$$g(x_a, x_a, i\eta) \neq 0; \tag{64}$$

but $g(x_a, x_a, i\eta)$, $a(i\eta)$ and $b(i\eta)$ are all real numbers, and therefore this requires the imaginary part of Equation (63) to be zero. For a controller that satisfies property P1 and for which $b(i\eta)$ is continuous and positive for $\eta \in (0, \infty)$, this is clearly impossible unless $\eta = 0$. Setting $\eta = 0$ in Equation (63), we find that the closed-loop poles must satisfy [we assume that $g_0(x_a, x_a, 0)$ exists, i.e., no rigid-body motion]

$$\frac{1}{\mu} + a(0)\, g_0(x_a, x_a, 0) = 0, \tag{65}$$

which is impossible for any positive value of μ if $a(0) \geqslant 0$, since $g(x_a, x_a, 0)$ is always positive. Hence collocation of the sensor and the actuator will cause the system to be stabilized for all controller gains when the controllers satisfy property P1 and have $a(0) \geqslant 0$, e.g., for the controllers listed in Equations (52)-(53). This result was introduced, though in a weaker form, by Balas [6].

V. SIMULATION RESULTS

We now show some simulation examples of the control design that we have discussed in this paper.

1. *Velocity Feedback Control*

We consider the system described by Equations (1)-(3) with the following parameters (assumed to be chosen in consistent units):

$$c = 2, \qquad L = 1, \qquad h_1 = 3, \qquad x_a - x_3 = 0.34567892,$$

$$x_a = 0.47654321. \tag{S1}$$

The transfer function of the controller is given by $\mathcal{T}_c(i\omega) = i\omega$. We will use configuration C1 for the simulation. For different values of the mass ratio M_r, the first nine open-loop natural frequencies $\beta_i = \omega_i / c$ are shown in Table 1.

From the results of the previous section, $M = c = 2$, and we are assured stability as long as $0 < \mu < 2$. For $M_r = 0$ the root loci corresponding to the

TABLE 1

Mode number	β_i			
	$M_r = 0$	0.5	1	5
1	1.192	0.875	0.715	0.3712
2	3.808	2.958	2.749	2.522
3	6.703	5.553	5.402	5.268
4	9.724	8.429	8.319	8.228
5	12.796	11.426	11.342	11.273
6	15.894	14.479	14.411	14.357
7	19.006	17.561	17.505	17.460
8	22.126	20.661	20.613	20.549
9	25.251	23.771	23.729	23.696

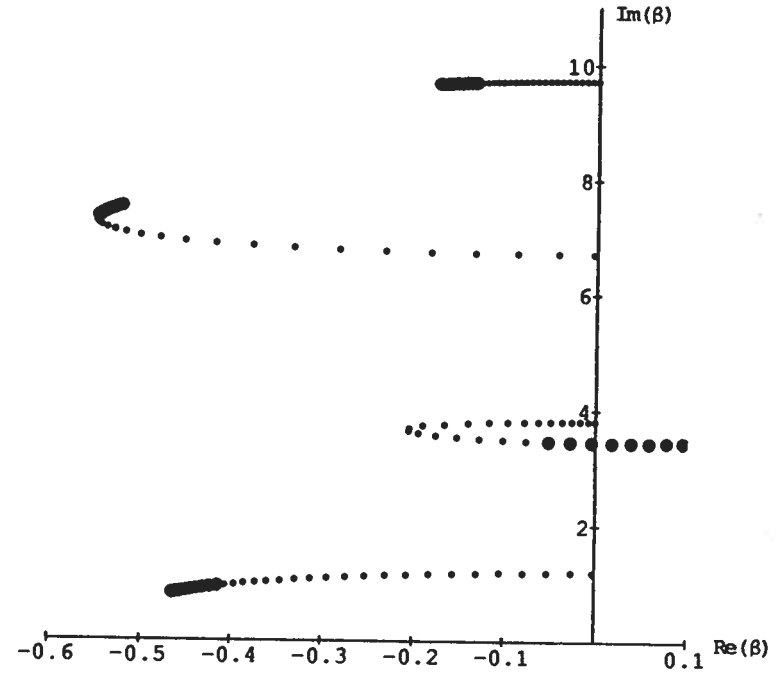

FIG. 3a. Velocity feedback control for elastically restrained system with $M_r = 0$: the lowest four closed-loop poles, showing $\bar{\beta}$ for different values of μ. Small circles indicate roots for $0 < \mu < M$; large circles, for $\mu > M$. The system is stable for $0 < u < M$.

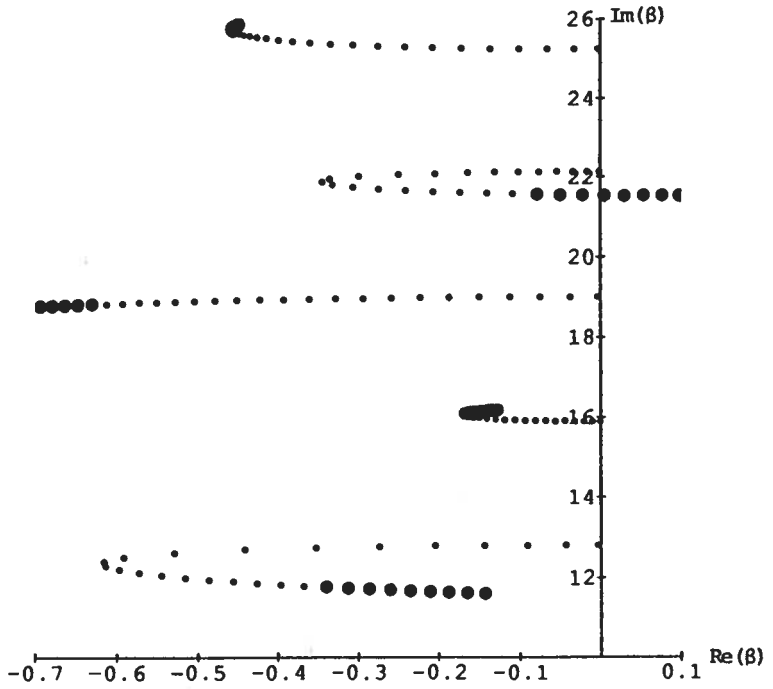

FIG. 3b. Velocity feedback control for elastically restrained system with $M_r = 0$: the next five closed-loop poles.

first nine poles are shown in Figures 3a and 3b for the upper half s-plane, using Equation (44). The roots $\bar{\beta}$ for different values of μ are shown. The location of the roots for all values of $0 < \mu < M$ are indicated by small circles. The large circles show the roots for $\mu > M$. We observe that the closed-loop poles, which all begin at $\mu = 0.01$, lie near the open-loop poles, which lie on the imaginary axis. The root loci of the poles corresponding to the second and eighth modes are seen to curve around and move into the right half s-plane, but only for $\mu > M$. For $0 < \mu < M$, all the closed-loop poles lie in the left half s-plane, as expected. Furthermore, on searching for the smallest value of μ for $n \in [0, 30]$ in Equation (61), we find that for $n = 16$ ($\bar{\beta}_n^* = 140.967i$), the value $\mu = 2.00237$ satisfies Equation (60). Thus the value $M = 2$ is a close approximation to $\mu^{\max}$. Figures 4, 5, and 6 show the root loci for values of M_r equal to 0.5, 1.0, and 5.0 respectively.

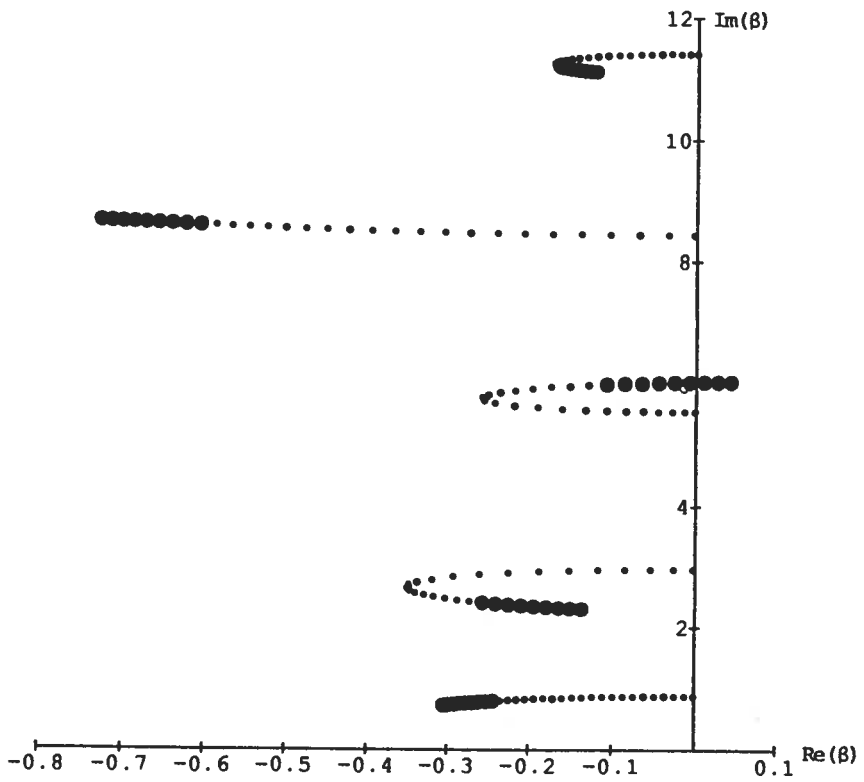

FIG. 4a. Velocity feedback control for elastically restrained system with $M_r = 0.5$: the lowest five closed-loop poles.

2. *Lead-Lag Compensator*

We model here a fixed end condition at one end, and use the following parameters (assumed to be in consistent units):

$$c = 2, \quad L = 1, \quad h_1 = 5000, \quad x_a - x_3 = 0.2, \quad x_a = 0.3854, \quad M_r = 0.5. \tag{S2}$$

Control is effected by a lead-lag compensator whose transfer function will be taken to be

$$\mathcal{T}_c(i\omega) = \frac{1 + \frac{1}{2}i\omega}{1 + \frac{1}{10}i\omega}.$$

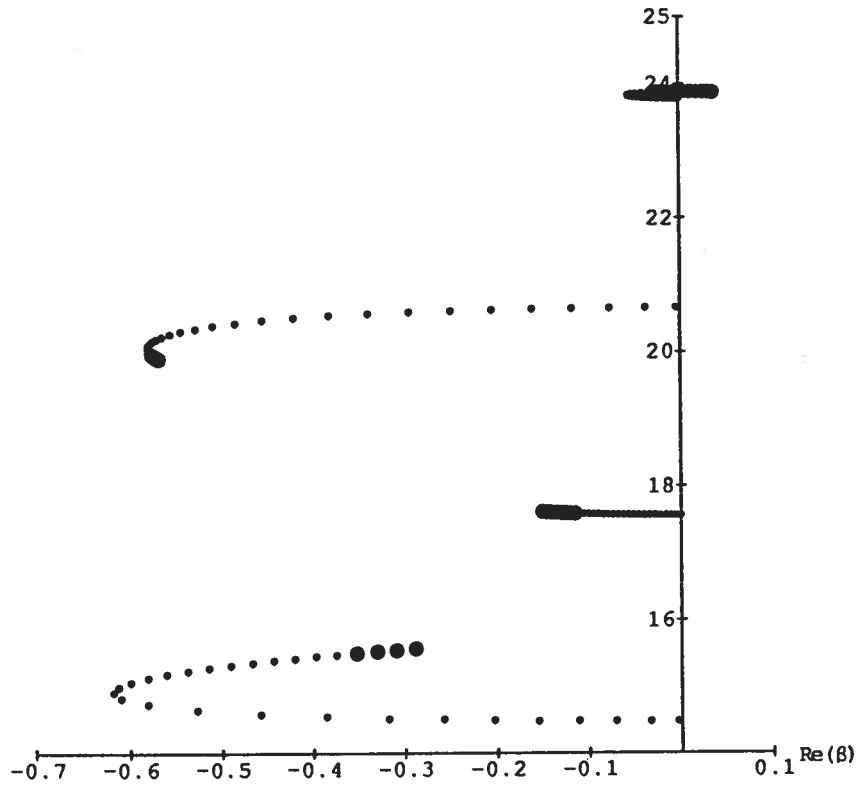

FIG. 4b. Velocity feedback control for elastically restrained system with $M_r = 0.5$: the next four closed-loop poles.

The sensor and actuator placements are taken to conform to configuration C1. We note that property P1 is satisfied. Figure 7 shows graphs of the left-hand side and right-hand side of Equation (54). We see that as long as

$$\mu < \frac{\eta_1^* b(\eta_1^*)}{a^2(\eta_1^*) + b^2(\eta_1^*)} \cdot c,$$

where $\eta_1^* = \pi/(x_a - x_3)$, Equation (54) cannot be satisfied and so the root locus must remain in the left half plane. The value of M (see Figure 7) is found to be (approximately) 3.1489. We note that as the distance $x_a - x_3$ decreases, η_1^* increases, thereby increasing the value of M, indicating that

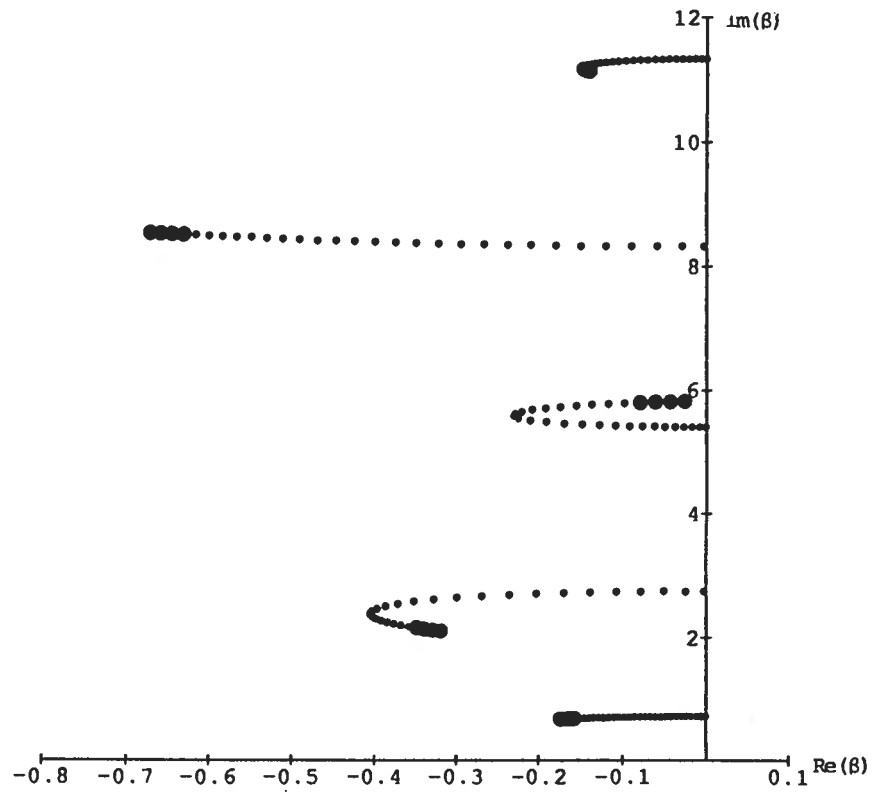

FIG. 5a. Velocity feedback control for elastically restrained system with $M_r = 1.0$: the lowest five closed-loop poles.

stability is ensured for larger and larger values of the gain μ. This is consistent with the results on collocated sensors and actuators.

Figure 8 shows the root loci determined using different values of μ. Again roots for values of $\mu < M$ are indicated by small circles. Roots for values of $\mu > M$ by large circles. The last large circle along the root locus corresponds to a value $\mu = 3.6$. The roots loci for all nine roots were found to lie in the left half s-plane for $0 < \mu < M$.

VI. CONCLUSIONS

In this paper we have shown that for systems of finite extent with tip inertias which are described by the one-dimensional wave equation, it is

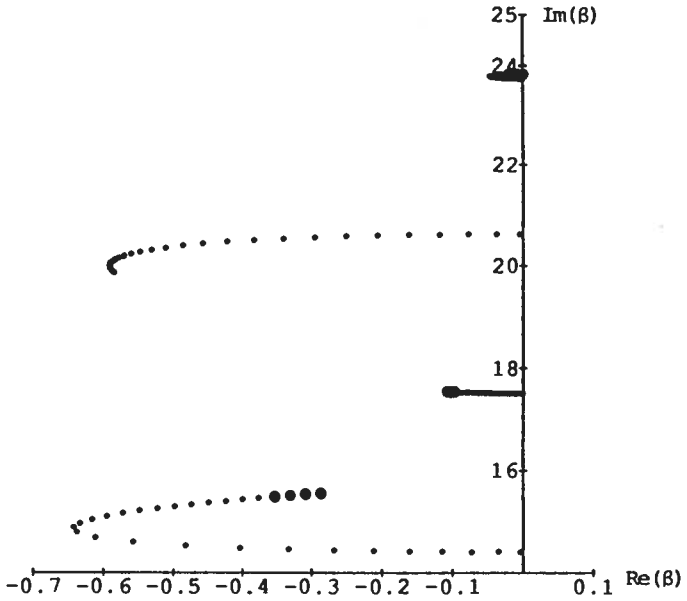

FIG. 5b. Velocity feedback control for elastically restrained system with $M_r = 1.0$: the next four closed-loop poles.

possible to have complete controllability when the sensors and actuators are noncollocated.

By properly locating the sensors and choosing appropriate time delays, the modal response of the system at time t at location x_a can be *exactly predicted* by measurements taken at three sensor locations at appropriate *prior times*. It is this property of perfect prediction that causes the effect of the signal delay time to be removed, leading to complete stabilizability using a finite-dimensional controller.

The control design offered in this paper is different from those proposed in the past (e.g. see [9, 4, 2, 5]) in that we use time-delayed inputs to the controller. The paper provides explicit lower bounds on the controller gains for which dampening of all modes is ensured. These bounds are expressed in terms of the actual locations of the sensors and the actuators and can be easily calculated. Simulation results are presented validating the control design methodology as well as the theoretically obtained bounds on the controller gains.

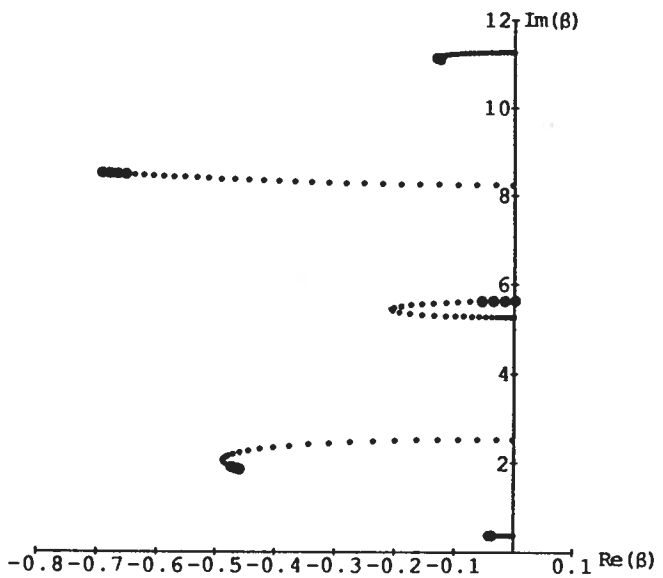

FIG. 6a. Velocity feedback control for elastically restrained system with $M_r = 5.0$: the lowest five closed-loop poles.

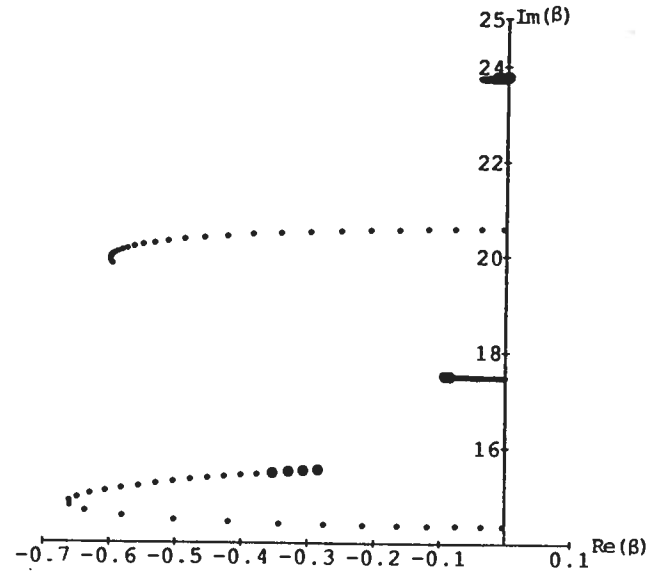

FIG. 6b. Velocity feedback control for elastically restrained system with $M_r = 5.0$: the next four closed-loop poles.

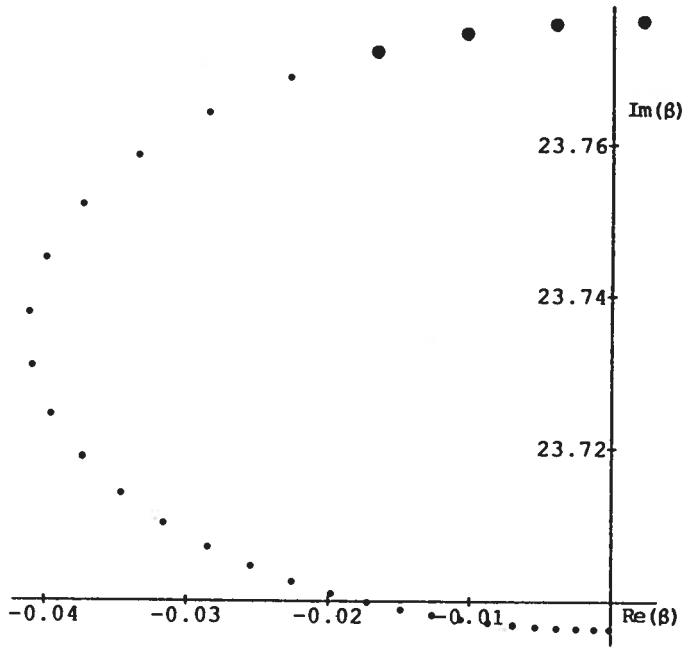

FIG. 6c. An expanded view of the ninth closed-loop pole in Figure 6b.

APPENDIX

We show here that

$$\left.\frac{d(\bar{\psi}-\bar{\phi})}{d\bar{\beta}}\right|_{\bar{\beta}\to \pm i\omega_k/c} = -\gamma_k,$$

where $\gamma_k > 0$.

Using Equations (15), we obtain

$$\operatorname{sech}^2\bar{\phi}\,\frac{d\bar{\phi}}{d\bar{\beta}} = \frac{1}{h_1} \tag{A.1}$$

and

$$\operatorname{sech}^2\bar{\psi}\,\frac{d\bar{\psi}}{d\bar{\beta}} = \frac{\bar{\beta}^2 L + M_r\bar{\beta}^2 - M_r^2\bar{\beta}^4 L}{\left(\bar{\beta}\sinh\bar{\beta}L + M_r\bar{\beta}^2\cosh\bar{\beta}L\right)^2}. \tag{A.2}$$

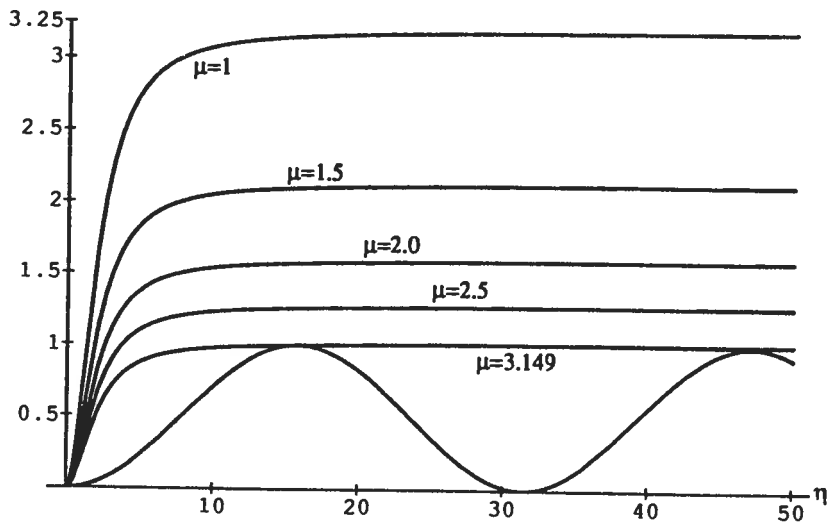

FIG. 7. Lead-lag compensator: the left-hand side of Equation (54), and its right hand side for different values of μ. For $0 < \mu < M \approx 3.149$, Equation (54) cannot be satisfied, ensuring stability.

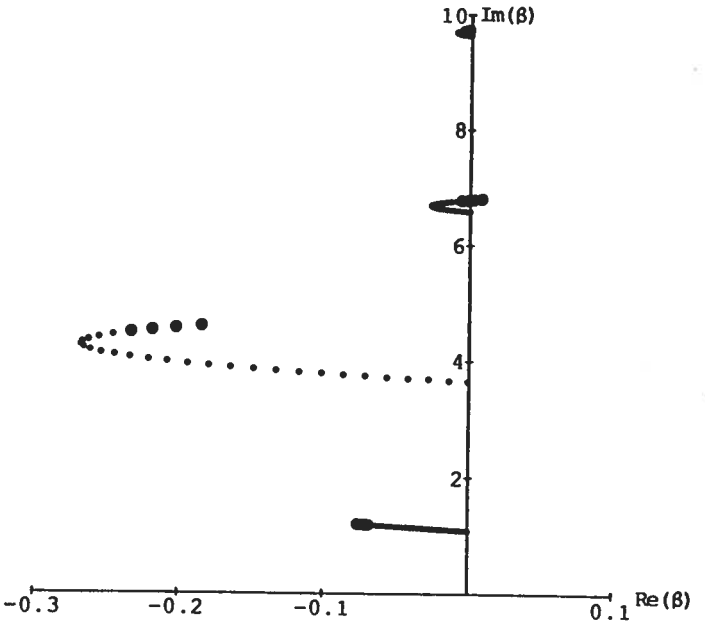

FIG. 8a. Lead-lag compensator for cantilever bar with $M_r = 0.5$: the lowest four closed-loop poles.

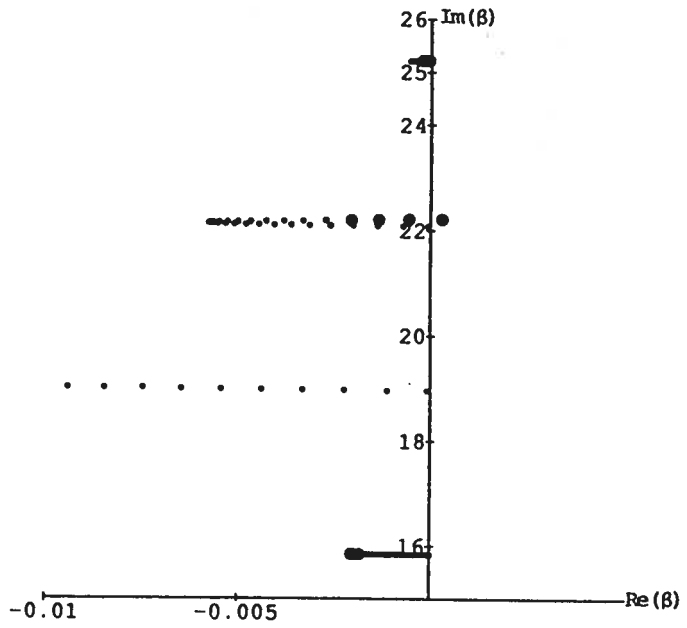

FIG. 8b. Lead-lag compensator for cantilever bar with $M_r = 0.5$: the next five closed-loop poles.

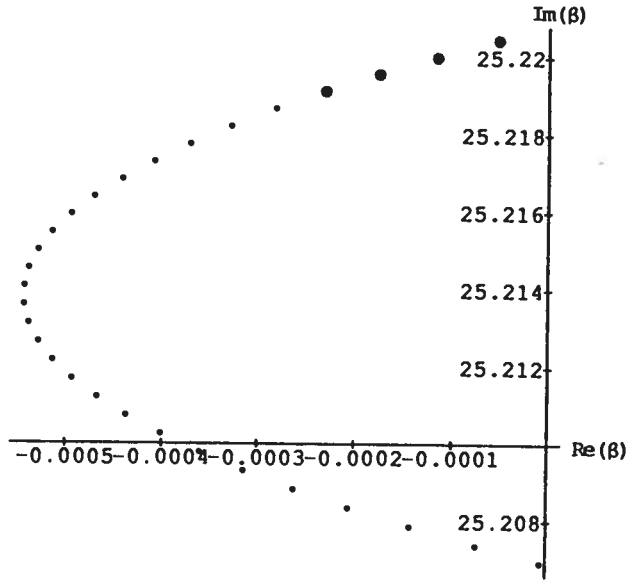

FIG. 8c. An expanded view of the ninth closed-loop pole of Figure 8b.

Taking the limit as $\bar{\beta} \to \pm i\omega_k/c$, and noting that $\psi_k = \phi_k \pm n\pi$, we obtain

$$\left.\frac{d(\bar{\psi}-\bar{\phi})}{d\bar{\beta}}\right|_{\bar{\beta}\to \pm i\omega_k/c} = -(\cos^2\phi)\left[\frac{\omega_k^2 L + M_r\omega_k^2 + M_r^2\omega_k^4 L}{(\omega_k \sin\omega_k L + M_r\omega_k^2\cos\omega_k L)^2} + \frac{1}{h_1}\right], \tag{A.3}$$

from which the result follows.

REFERENCES

1 T. Bailey and J. Hubbard, Distributed piezoelectric-polymer active vibration control of a cantilever beam, *J. Guidance and Control* 8(5):605–611 (Sept.–Oct. 1985).

2 M. Balas, Feedback control of linear distributed parameter systems: What can be accomplished with a finite-dimensional controller?, Plenary Lecture, in *Proceedings of the IFAC Symposium on Large Scale Systems*, Warsaw, 1983.

3 M. Balas and C. R. Johnson, Adapative control of distributed parameter systems: The ultimate reduced order problem, in *Proceedings of the 18th IEEE Control and Decision Conference*, Ft. Lauderdale, FL., 1979.

4 M. Balas, Feedback control of flexible systems, *IEEE Trans. Automat. Control* AC-23(4):673–679 (1978).

5 M. Balas, in *Proceedings of the NASA Workshop on Identification and Control of Flexible Space Structures*, JPL Publication 85-29, 1985, Vol. 2, pp. 111–132.

6 M. Balas, Direct velocity feedback control of large space structures, *J. Guidance and Control* 2(3):252–253 (June 1979).

7 A. G. Butkovskiy, *Structural Theory of Distributed Systems*, Ellis Horwood, New York, 1983.

8 C. A. Desoer and M. Vidyasagar, *Feedback Systems: Input-Output Properties*, Academic, 1975, pp. 182–187.

9 J. S. Gibson, An analysis of optimal modal regulation: Convergence and stability, *SIAM J. Control Optim.* 19(5):686–707 (Sept. 1981).

10 L. Meirovitch and H. Oz, Modal space control of gyroscopic systems, *J. Guidance and Control* 3(2):140–150 (1980).

11 D. Mingori, J. S. Gibson, P. Blelloch, and A. Adamian, Control of a flexible space antenna: A finite dimensional perspective based on distributed parameter theory, presented at Workshop on Identification and Control of Flexible Structures, San Diego, 4–6 June 1984.

12 I. Stackgold, *Green's Functions and Boundary Value Problems*, Wiley, 1979.

13 B. Yang and C. D. Mote, Vibration Control of Band Saws: Theory and Experiment, Report, Dept. of Mechanical Engineering, Univ. of California, Berkeley, 1989.

14 F. E. Udwadia, Control of continuous systems, in *Proceedings of the XV*th *SECTAM Conference*, Atlanta, 23–25 Mar. 1990.

15 F. E. Udwadia, Noncollocated point control of nondispersive continuous systems using time delays, *Appl. Math. Comput.* 42(1)23–63 (1991).